JTTEE5 14:85-90
DOI: 10.1361/10599630522422
1059-9630/$19.00 © ASM International

Influence of Hydrogen on the Microstructure of Plasma-Sprayed Yttria-Stabilized Zirconia Coatings

J.F. Bisson, C. Moreau, M. Dorfman, C. Dambra, and J. Mallon

(Submitted December 12, 2003; in revised form May 24, 2004)

The influence of secondary hydrogen and current on the deposition efficiency (DE) and microstructure of yttria-stabilized zirconia (YSZ) coatings was evaluated. To better understand the influence of the spray process on coating consistency, a YSZ powder, −125 +44 μm, was sprayed with nitrogen/hydrogen parameters and a 9 MB plasma gun from Sulzer Metco. DE and coating porosity, which were produced using two different spray gun conditions yielding the same input power, were compared. Amperage was allowed to vary between 500 and 560 A, and hydrogen was adjusted to maintain constant power, while nitrogen flow was kept at a fixed level. Several power conditions, ranging from 32 to 39 kW, were tested. Different injection geometries (i.e., radial with and without a backward component) were also compared. The latter was found to produce higher in-flight temperatures due to a longer residence time of the powder particles in the hotter portion of the plasma. Porosity was based on cross-sectional micrographs. In-flight particle temperature and velocity measurements were also carried out with a special sensor for each condition. Test results showed that DE and coating density could vary significantly when a different hydrogen flow rate was used to maintain constant input power. On the other hand, DE was found to correlate very well with the temperature of the in-flight particles. Therefore, to obtain more consistent and reproducible DE and microstructures, it is preferable to maintain the in-flight particle temperature around a constant value instead of keeping a constant input power by adjusting the secondary hydrogen flow rate.

Keywords particle characteristics, plasma spraying, process control, thermal barrier coating, zirconia

1. Introduction

Improving the consistency of thermal barrier coatings (TBCs) is an important goal for the industry. Indeed, TBCs are used today in increasingly demanding and critical applications requiring highly reliable and consistent coating properties. Combustion liners and transition pieces are examples of parts currently protected by plasma-sprayed TBCs for ensuring a safe and reliable use of gas turbine components (Fig. 1). Short-term (Ref 1, 2) and long-term (Ref 3, 4) plasma gun instabilities arising from anode wear are among the various factors that contribute to coating degradation. These instabilities result in a variation in coating microstructure and deposition efficiency (DE). Indeed, anode wear is known to cause power drifts in the plasma gun, which implies varying heat and kinetic energy transfers to the injected particles (Ref 5, 6).

Several strategies can be used to compensate for changes in the spray conditions arising from the wear of the electrodes (Ref 7). Maintaining some key in-flight parameters, such as the average in-flight temperature and velocity (Ref 8), has proven to be a very effective control approach, but, up to now, only a limited number of spray booths have been equipped with sensors that can measure such in-flight particle parameters. Hence, other control approaches, consisting of maintaining fixed values for some spray gun parameters that are correlated with the temperature and velocity of the particle jet, and that are more readily measured than the in-flight parameters, have been used. The input power and the net power (i.e., the fraction of the input power that goes into the plasma flame) are two spray gun variables that are known to correlate with the in-flight particle characteristics and that can be readily measured using commercial plasma spray consoles. Both can easily be controlled. For instance, adjusting the input current or the secondary gas (e.g., the hydrogen flow) can compensate for any drift in the input power. Both approaches are used in industry. Some gun manufacturers have recognized these process instabilities and have previously developed spray parameters with fixed secondary gas conditions to maintain a constant particle or flame temperature. Closed-loop controllers have also been engineered to allow input power, and primary and secondary gas levels to be fixed. However, the emergence of sensor technologies in thermal spraying has made it possible to better understand the sensitivity of secondary gas levels on particle temperature, and its impact on yttria-stabilized zirconia (YSZ) microstructure and DE.

This study aimed at evaluating a control strategy, consisting of maintaining the input power, to ensure a consistent TBC microstructure and DE. First, the YSZ powder feedstock used during these experiments is described. Then, the spray conditions

The original version of this article was published as part of the ASM Proceedings, *Thermal Spray 2003: Advancing the Science and Applying the Technology,* International Thermal Spray Conference (Orlando, FL), May 5-8, 2003, Basil R. Marple and Christian Moreau, Ed., ASM International, 2003.

J.F. Bisson and **C. Moreau,** National Research Council of Canada, Boucherville, Québec, Canada; and **M. Dorfman, C. Dambra,** and **J. Mallon,** Sulzer Metco (US) Inc., Westbury, NY. Contact e-mail: Christian.moreau@cnrc-nrc.gc.ca.

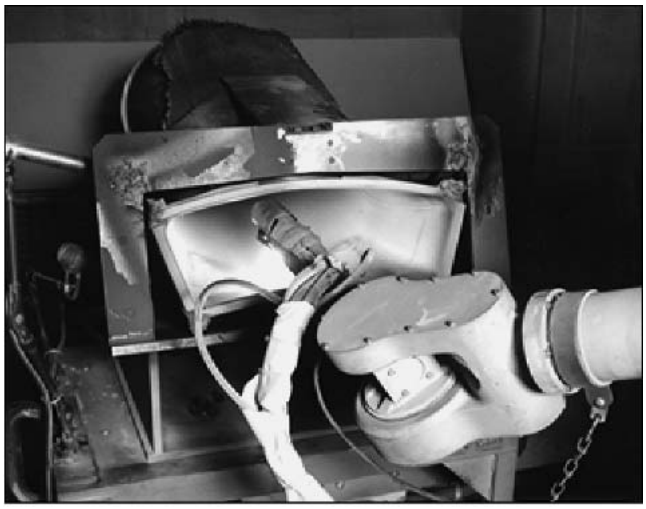

(a)

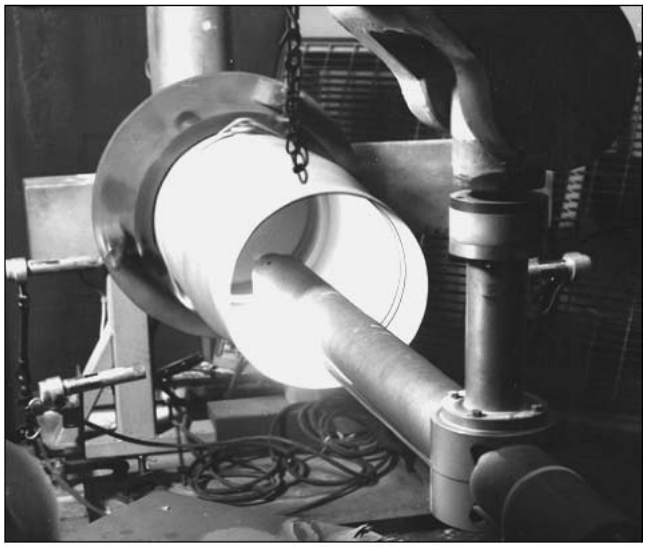

(b)

Fig. 1 Robotic application of TBC by plasma spraying in (a) the transition piece and (b) the combustion liner. (Photo permission of Jim Clare, General Electric, Beaumont, TX)

selected to perform this work are presented. Next, the experimental procedure used to perform in-flight particle diagnostics is described. Particle diagnostics were performed to understand the variations in the coating porosity and DE observed at constant input power. In-flight particle diagnostics were performed with the DPV-2000 sensor (Tecnar Automation Ltd., St-Bruno, Canada) to relate changes in the coating to changes in the in-flight particle physical parameters (i.e., the particle velocity and temperature). Finally, the results in DE and coating porosity are presented. Differences are interpreted based on the in-flight diagnostic results.

2. Evaluation of the Feedstock Material

The powder used in this work is a homogeneous oven spherical particle (HOSP) partially stabilized yttria-zirconia material,

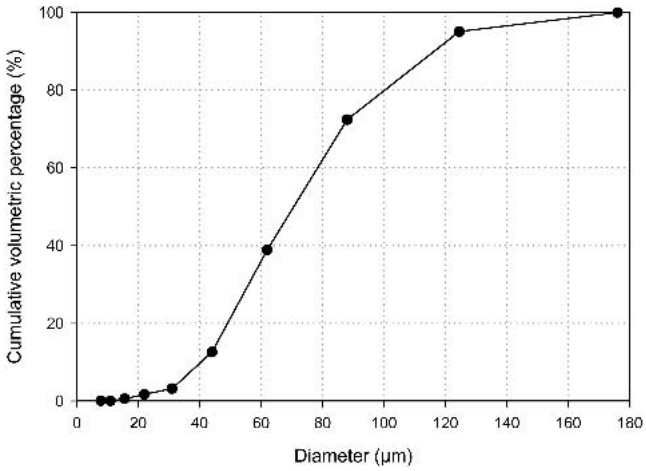

Fig. 2 Cumulative particle size distribution in volumetric percentage obtained by employing the Microtrac method

Table 1 Quantitative elemental analysis of the HOSP powder using inductively coupled plasma

Elements	wt.%
A1	0.02
Ca	0.04
Ce	0.01
Fe	0.01
HF	1.48
Mg	<0.01
Na	0.07
Si	0.14
Th	0.009
Ti	0.02
U	0.021
Y	5.96
Zr	66.66
Organic solids	0.05

with a relatively coarse (120-325 mesh) particle size distribution. The particle size distribution, obtained using Microtrac (Microtrac, Inc., Montgomeryville, PA) analysis, ranges from 20 to 120 μm, as shown in Fig. 2. An inductively coupled plasma technique was used for the elemental analysis of powder samples. The results are shown in Table 1. Scanning electron microscopy (SEM) using secondary electrons was used to examine the surface and the cross section of powder particles. As seen in Fig. 3, they consist of spherical plasma-densified particles. The cross sections of the particles were obtained by casting a powder sample into a standard mounting epoxy, followed by polishing. An examination of particle cross sections enabled an evaluation of the powder density and the extent of particle sintering during manufacturing. As shown in Fig. 4 and 5, most of the particles were almost completely remelted during the sintering phase of the manufacturing process except for some coarser particles, of which the core is still in the agglomerated form. This property reduces the probability that a particle breaks apart during its interaction with the plasma flame. Moreover, the rounded shape of the feedstock material favors a better flow (called flowability) in the injection line.

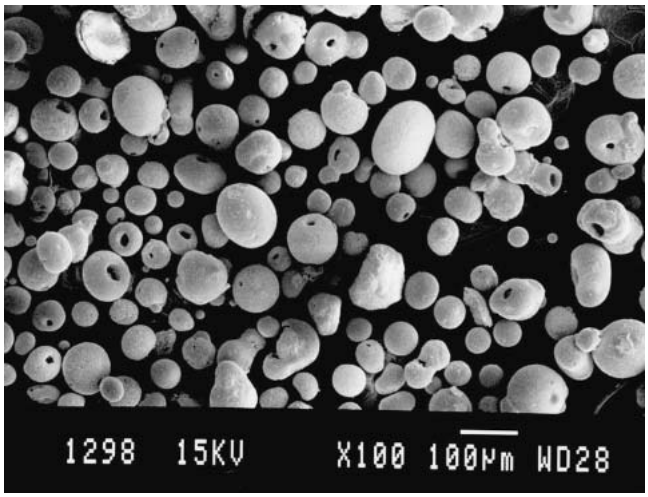

Fig. 3 Surface of HOSP powder particles

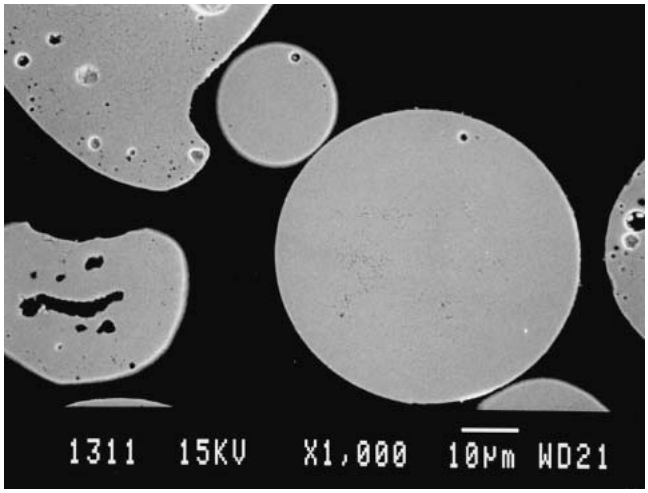

Fig. 4 Cross section of YSZ HOSP powder particles

3. Experimental Procedure

3.1 Spray Conditions

The YZP HOSP powder was sprayed using a 9 MB plasma gun from Sulzer Metco (Westbury, NY). Nitrogen and hydrogen were used as the plasma gas mixture. Two different powder feed ports were used. The P-injection port provides perpendicular (vertical) injection of the particles into the plasma, whereas the B-injection port has a backward injection component that allows the particles to remain for a longer period of time in the hotter part of the plasma. The backward angle is around 8°. With the P-injection port, three power conditions were used (36, 37.5, and 39 kW), whereas two power conditions (32 and 39 kW) were tested with the B-injection port. Each power level was achieved using two sets of spray conditions having different levels of current and hydrogen flow rate (i.e., high-hydrogen/low-current and low-hydrogen/high-current). Spraying conditions are summarized in Table 2. All other spraying parameters were kept constant throughout this work.

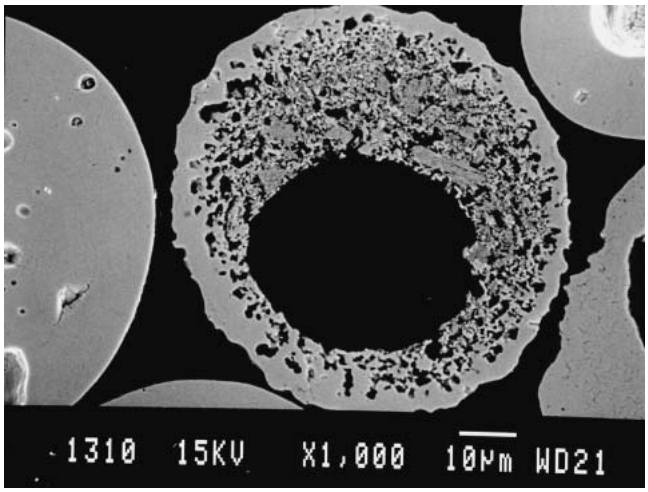

Fig. 5 Cross section of YSZ HOSP powder particles. Some large particles were not fully molten during processing.

Table 2 Spraying conditions

Condition	Current (I), A	H_2, L/min	Input power, kW	Powder feed port
1	530	7.1	39	P
2	530	2.8	36	P
3	520	7.1	37.5	P
4	550	2.8	37.5	P
5	530	4.7	36	P
6	560	4.7	39	P
7	530	6.2	38	B
8	430	6.2	32	B
9	475	1.9	32	B
10	560	2.0	38	B

Note: The nitrogen and the powder carrier gas flow rates were maintained at 41.5 and 4 L/min, respectively.

During spraying, the samples were continuously cooled down with an air jet to maintain the surface temperature at between 125 and 175 °C. The steady-state substrate temperature was measured using pyrometric measurements with a Micron pyrometer, which is sensitive in the wavelength region of 8 to 14 µm. The samples were 7.5 cm^2 coupons. The transverse gun speed was 75 cm/s with a vertical jump of 3.2 mm after each horizontal scan to deposit a thickness of about 25 µm per pass.

Both the input power and net plasma power were measured for each spraying condition. The input power is taken as the product of the current and voltage in a specific spray condition. The net power is obtained by subtracting the input power from the thermal losses. Thermal losses are estimated by measuring the temperature difference between the cooling water flowing in and out of the torch and by using the specific heat and flow rate of the cooling water. This yields the amount of enthalpy flowing out of the plasma plume.

3.2 In-Flight Diagnostics

Before spraying the coatings, in-flight particle diagnostics were performed using the DPV-2000 sensor (Ref 9, 10). This sensor enables in-flight measurements of the temperature, ve-

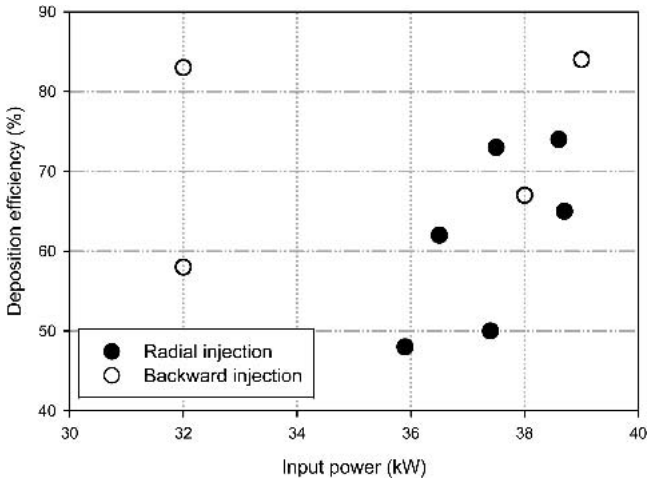

Fig. 6 Deposition efficiency versus input power. The error on the DE values was ±3%.

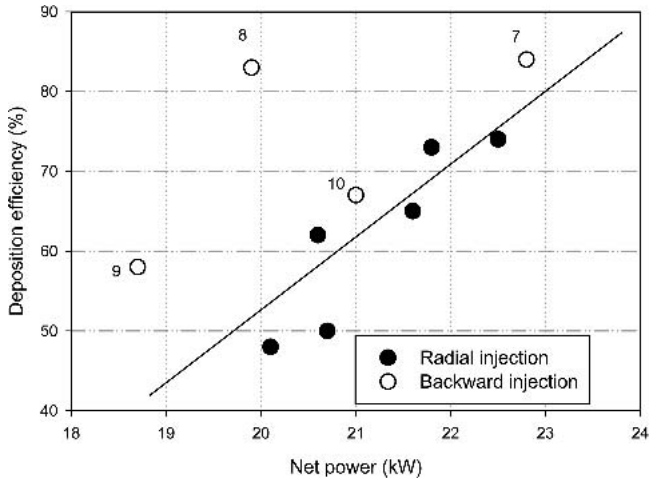

Fig. 7 Deposition efficiency versus net power. Numbers indicated for the backward injection correspond to the spray conditions given in Table 3. The error on the DE values was ±3%.

Table 3 Summary of the diagnostic results and DE for all the tested conditions and thermal efficiency

Condition	Powder feed port	Current (*I*), A	H_2, L/min	Voltage, V	Input, kW	Net, kW	Gun efficiency (η), %	Temperature (*T*), °C	Velocity (*V*), m/s	DE, %
1	P	530	7.1	72.9	38.6	22.5	0.560	2665	98	74
2	P	530	2.8	67.7	35.9	20.1	0.580	2541	90	48
3	P	520	7.1	72.1	37.5	21.8	0.550	2686	94	73
4	P	550	2.8	68.0	37.4	20.7	0.565	2550	92	50
5	P	530	4.7	68.9	36.5	20.6	0.560	2640	98	62
6	P	560	4.7	69.1	38.7	21.6	0.605	2628	99	65
7	B	530	6.2	73.6	38.0	23.6	0.620	2840	92	84
8	B	430	6.2	74.4	32.0	19.8	0.595	2804	82	83
9	B	475	1.9	67.3	32.0	19.0	0.560	2624	78	58
10	B	560	2.0	67.9	38.0	21.3	0.580	2651	86	67

Note: η, ratio of net power to input power. Better η is favored by higher hydrogen flow and lower current.

locity, and diameter of the individual sprayed particles. Diagnostics were performed at the same standoff distance (10 cm) as that used to spray the coatings. The measurements provided herein were obtained in the middle of the particle jet, where the particle flow rate was found to be maximum. In fact, an analysis of two-dimensional scans in the particle jet indicated that the average value obtained at the center of the particle jet was almost identical to the average value of the whole particle jet. This was the case because the particle flow rate dropped rapidly away from the center before any significant changes in velocity or temperature were noticed. To reduce powder consumption, low powder feed rates was used for diagnostics (5-10 g/min). The loading effect was evaluated beforehand and was found to induce drops of 75 °C and 5 to 10 m/s, respectively, in the in-flight temperature and velocity when the feed rate was increased to 45 g/min.

4. Results and Discussion

4.1 Deposition Efficiency

DE is plotted as a function of input power in Fig. 6. The data are scattered and only moderately correlated with the input power, as conditions having similar power levels were sometimes found to display very different DEs. A higher correlation was obtained with the net power (Fig. 7), especially when the P-injection port was used. This higher correlation likely arises from the fact that the variations in DE that were observed at similar input power (e.g., conditions 1-4, 2-3, 5-8, and 6-7) were due to the higher thermal efficiencies (η = net power/input power) observed for spray conditions using higher H_2 flow and lower current values (Ref 11). A higher enthalpy in the plasma flame will likely produce a larger fraction of melted particles and, generally, a higher DE. The thermal efficiency values are shown in Table 3. However, note that the net power does not track the effect of changes in the injection conditions, which could be caused, for example, by injector wear (Ref 12). This is illustrated by the higher DE, which was obtained for the exact same spray gun parameters, when the P-injection port was replaced by the B-injection port.

With the backward injection (B-injection port), the correlation between DE and net power is quite poor. DEs were significantly higher when high hydrogen flow rates were used (i.e., conditions 7 and 8). This is likely related to the better heat transfer to the particles associated with the higher thermal conductivity of hydrogen-rich plasmas (Ref 13). This effect is probably more important when using backward injection instead of radial injection because the particles travel in hotter plasma regions in the former case.

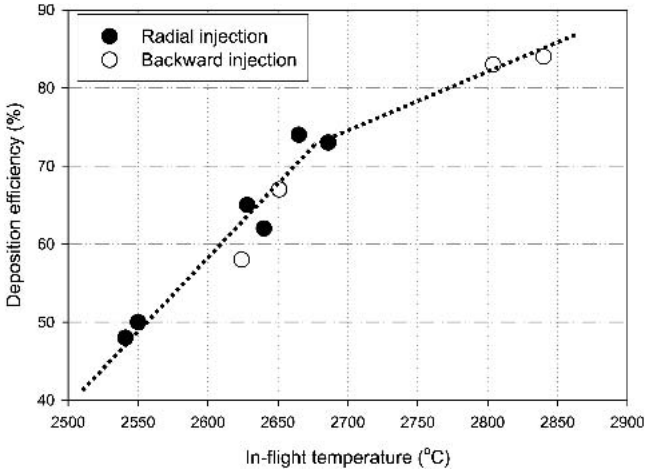

Fig. 8 Deposition efficiency as a function of in-flight temperature. The error on the DE values was ±3%.

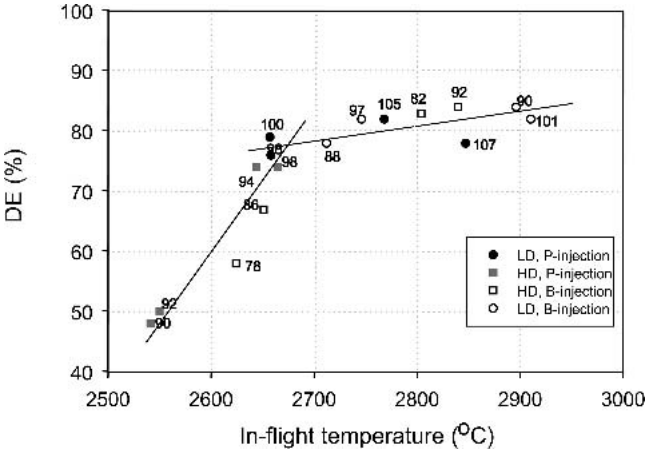

Fig. 9 Deposition efficiency as a function of in-flight temperature for two different zirconia powders. The values shown near each data point are the average in-flight velocity. LD, low-density powder; HD, high-density powder. The error on the DE values was ±3%. Based on data from Ref 14

A plot of DE versus average in-flight particle temperature is shown in Fig. 8. The observed correlation between the average in-flight particle temperature and DE indicates that the higher DE obtained with the B-injection port arises mainly from the higher average particle temperature that can be reached using this injector. Indeed, all of the data points seem to fall on a single curve with very little data scattering, regardless of which injector was used. Below 2700 °C, DE is found to increase by 20% for a 100 °C temperature step. Above 2700 °C, the variation of DE with temperature becomes less pronounced. As illustrated in Fig. 9, a similar trend was observed with another zirconia powder having a lower density, confirming that the DE is strongly linked to the actual temperature of the in-flight particles (Ref 14).

The correlation between DE and in-flight temperature is better than with the net power. Moreover, the influence of injection on DE is well accounted for by the in-flight temperature.

4.2 Microstructure and Porosity

The microstructure of the coatings can be interpreted with respect to the in-flight particle characteristics, in particular the in-flight temperature. Coatings produced at similar input power with different current-hydrogen combinations were found to be very different. SEM photographs of cross sections of two coatings produced at 38 kW at high (condition 7, Fig. 10) and low (condition 10, Fig. 11) hydrogen flow rates clearly show that the coating produced at a higher hydrogen concentration is significantly denser than the other coating. The denser coating corresponds to higher in-flight temperature (2840 versus 2650 °C). At 2840 °C, most particles are melted, so that each splat covers more easily the surface topography onto which it flattens. Moreover, at that higher in-flight temperature there is normally a lower number of unmolten or partially molten particles embedded in the coating. These two factors favor the deposition of low-porosity coatings. However, at 2650 °C, many particles are unmolten or partially molten, so that some of the initial porosity of the feedstock can be retained in the coating. Moreover, the impinging particles do not flatten as well, which leaves some air trapped underneath the splat. Note that using the P-injection port (condition 1, Fig. 12) instead of the B-injection port (condition 7, Fig. 11) at similar spray gun parameters yielded a more porous coating for a similar reason (P-injection port 2665 °C; B-injection port 2840 °C).

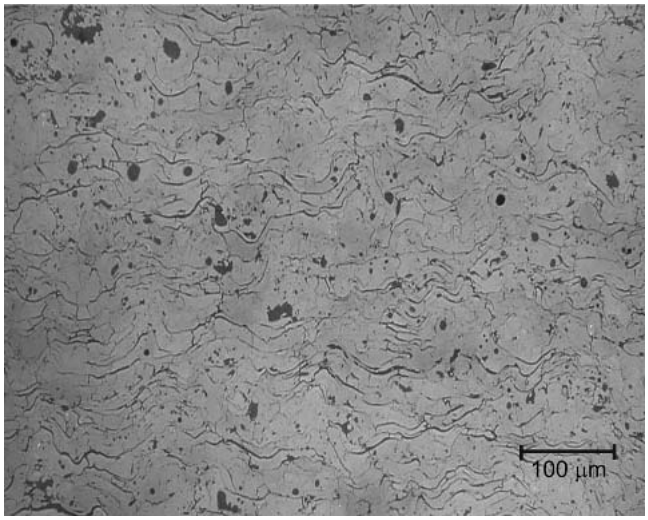

Fig. 10 Cross section of the coating obtained at 38 kW with high hydrogen (condition 7) with the B-injection port

5. Conclusion

The influence of secondary hydrogen and current on the DE and microstructure of YSZ coatings was evaluated. A YSZ powder was sprayed with nitrogen/hydrogen parameters using a Sulzer Metco 9 MB gun. DE and coating porosity produced using different spray gun conditions yielding a similar input power were compared. Similar values of input power could be obtained by compensating for a rise in current by decreasing the hydrogen flow.

Significant discrepancies in porosity and DE were sometimes found in coatings produced with different spray parameters yielding similar input powers. The higher hydrogen flow condition was found to produce higher DE and a denser coating mi-

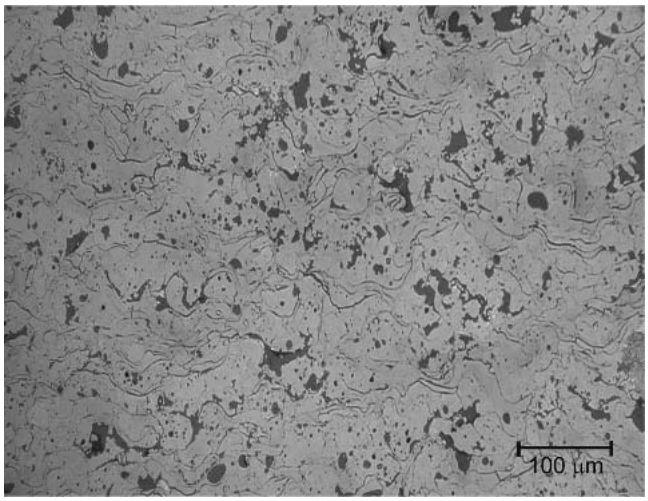

Fig. 11 Cross section of the coating produced at 38 kW with low hydrogen (condition 10) with the B-injection port

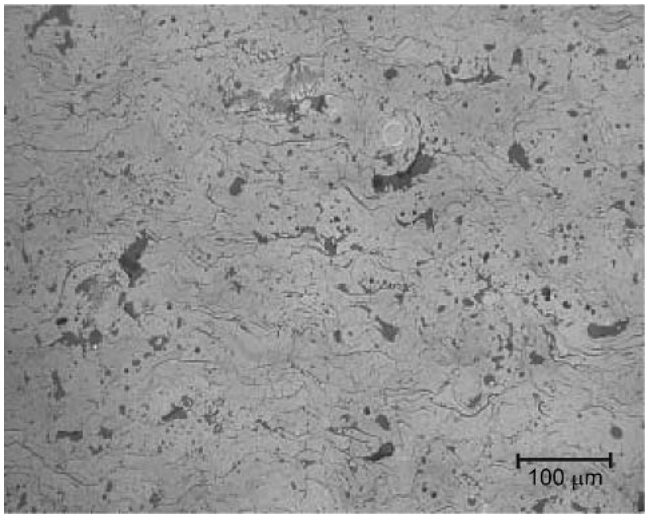

Fig. 12 Cross section of the coating obtained at 38 kW with high hydrogen (condition 1) with the P-injection port

crostructure. Differences in DE and porosity were linked to the higher plasma enthalpy and heat transfer to the particles that could be achieved at a higher hydrogen-lower current condition. Hence, a better correlation was found between the coating DE and the net power in the plasma.

Moreover, changing the injection conditions by using backward injection instead of vertical injection was found to produce significant changes in DE and microstructure. These results illustrate that the net power cannot follow eventual changes in the injection conditions due to injector erosion.

The average in-flight particle temperature was found to correlate very well with DE, regardless of the particular choice of hydrogen-current combination or of the way particles were injected into the plasma.

In view of these results, the control of a plasma spray process by maintaining the input power does not seem to be the best approach to ensure consistency in the coating DE and microstructure. Maintaining the net power is a better approach, but this approach does not track the eventual changes in the injection conditions. The control of the physical characteristics of the particle jet, such as the in-flight temperature and velocity, seems to be the most effective approach to ensure consistency for the production of TBCs.

Acknowledgments

The authors are grateful to Sylvain Bélanger of NRC for operating the spraying booth and to Mario Lamontagne for performing particle diagnostics, Eric Poirier for metallographic sample preparation, and Michel Thibodeau for microstructure characterization by SEM.

References

1. J.F. Bisson, B. Gauthier, and C. Moreau, Effect of Plasma Fluctuations on In-Flight Particle Parameters, *J. Therm. Spray Technol.,* Vol 12 (No. 1), 2003, p 38-43
2. J.F. Bisson and C. Moreau, Effect of Plasma Fluctuations on In-Flight Particle Parameters: Part II, *Tagungsband Conference Proceedings,* E. Lugscheider, Ed., DVS Deutscher Verband für Schweissen, Essen, Germany, 2002, p 666-671
3. L. Leblanc, C. Moreau, P. Gougeon, and J. Xi, Long Term Stability of Plasma Spraying: Study on the Evolution of the In-Flight Particle State, Coating Microstructure, Voltage and Acoustic Signatures, *Tagungsband Conference Proceedings,* E. Lugscheider and P.A. Kammer, Ed., DVS Deutscher Verband für Schweissen, Dusseldorf, Germany, 1999, p 306-311
4. L. Leblanc and C. Moreau, Study of the Long-Term Stability of Plasma Spraying, *Thermal Spray: Surface Engineering via Applied Research* (Montréal, Québec, Canada), May 8-11, 2000, C.C. Berndt, Ed., ASM International, 2000, p 1233-1239
5. M. Vardelle, A. Vardelle, P. Fauchais, and M.I. Boulos, Plasma-Particle Momentum and Heat Transfer: Modelling and Measurements, *AIChE J.,* Vol 29 (No. 2), 1983, p 236-243
6. J.R. Fincke, R.L. Williamson, and C.H. Chang, Plasma Spraying of Functionally Graded Materials: Measured and Simulated Results, *Thermal Spray: Surface Engineering via Applied Research* (Montréal, Québec, Canada), May 8-11, 2000, C.C. Berndt, Ed., ASM International, 2000, p 141-148
7. C. Moreau, Towards a Better Control of Thermal Spray Processes, *Thermal Spray: Meeting the Challenges of the 21st Century* (Nice, France), May 25-29, 1998, C. Coddet, Ed., ASM International, 1998, p 1681-1693
8. C. Moreau, P. Gougeon, M. Lamontagne, V. Lacasse, G. Vaudreuil, and P. Cielo, On-Line Control of the Plasma Spraying Process by Monitoring the Temperature, Velocity, and Trajectory of the In-flight Particles, *Thermal Spray Industrial Applications,* (Boston, MA), June 20-24, 1994, C.C. Berndt and S. Sampath, Ed., ASM International, 1994, p 431-436
9. J. Blain, F. Nadeau, L. Pouliot, C. Moreau, P. Gougeon, and L. Leblanc, Integrated Infrared Sensor System For On-Line Diagnostics of Particles Under Thermal Spraying Conditions, *Surf. Eng.,* Vol 13, 1997, p 420-424
10. Tecnar Automation Ltd Home Page, www.tecnar-automation.com (accessed May 2004)
11. R. Ramasamy, V. Selvarajan, K. Perumal, and G. Shanmugavelayutham, An Attempt to Develop Relation for the Arc Voltage in Relation to the Arc Current and Gas Flow Rate, *Vacuum,* Vol 59, 2000, p 118-125
12. K. Seeman, A. Fisher, and E. Lugscheider, Influence of Noise Factors at Atmospheric Plasma Spraying, *Tagungsband Conference Proceedings,* E. Lugscheider, Ed., DVS Deutscher Verband für Schweissen, Essen, Germany, 2002, p 1007-1010
13. M. Boulos, P. Fauchais, and E. Pfender, *Thermal Plasmas: Fundamental and Applications,* Vol 1, Plenum Press, 1994, p 302, 309
14. J.-F. Bisson, C. Moreau, M. Dorfman, C. Dambra, and J. Mallon, Behavior and Characterization of Two 7-8 wt% Yttria-Stabilized Zirconia Powders and Coatings Produced Using Plasma Spray Deposition, *Thermal Spray 2003: Advancing the Science and Applying the Technology* (Orlando, FL), May 5-8, 2003, B.R. Marple and C. Moreau, Ed., ASM International, 2003, p 1583-1589